Editors' Suggestion | Featured in Physics

Boosting Thermal Conductivity by Surface Plasmon Polaritons Propagating along a Thin Ti Film

Dong-min Kim,[1,2] Sinwoo Choi,[1,2] Jungwan Cho,[3] Mikyung Lim,[4,*] and Bong Jae Lee[1,2,†]
[1]Department of Mechanical Engineering, Korea Advanced Institute of Science and Technology, Daejeon 34141, South Korea
[2]Center for Extreme Thermal Physics and Manufacturing, Korea Advanced Institute of Science and Technology, Daejeon 34141, South Korea
[3]School of Mechanical Engineering, Sungkyunkwan University, Suwon 16419, South Korea
[4]Nano-Convergence Manufacturing Systems Research Division, Korea Institute of Machinery and Materials, Daejeon 34103, South Korea

(Received 22 July 2022; accepted 1 March 2023; published 26 April 2023)

We experimentally demonstrate boosted in-plane thermal conduction by surface plasmon polaritons (SPPs) propagating along a thin Ti film on a glass substrate. Due to the lossy nature of metal, SPPs can propagate over centimeter-scale distances even along a supported metal film, and the resulting ballistic heat conduction can be quantitatively validated. Further, for a 100-nm-thick Ti film on a glass substrate, a significant enhancement of in-plane thermal conductivity compared to bulk value (~25%) is experimentally shown. This Letter will provide a new avenue to employ SPPs for heat dissipation along a supported thin film, which can be readily applied to mitigate hot-spot issues in microelectronics.

DOI: 10.1103/PhysRevLett.130.176302

Nanoscale thin films often exhibit a size effect on thermal conductivity because their thicknesses are less than the lengths of phonon or electron mean free paths [1,2]. Reduced thermal conductivity prevents heat dissipation from hot spots, compromising device performance. It has been shown that surface electromagnetic waves, which propagate longer than primary heat carriers [3–9], can compensate for the classical size effect.

Surface phonon polaritons (SPhPs) can carry heat and thus enhance the dielectric film thermal conductivity [10–12]. Several earlier studies have investigated the thermal transport of suspended dielectric membranes via SPhPs [5,6,9,13]. Chen *et al.* [5] initially proposed that SPhPs can enhance the in-plane thermal conductivity of a 40-nm-thick SiO_2-suspended membrane by more than 100%. This is because SPhPs propagate orders of magnitude further than acoustic phonons in a SiO_2 membrane [7,14]. Subsequently, Tranchant *et al.* [9] measured the in-plane thermal conductivity of the suspended SiO_2 membrane with respect to its thickness and width. Their results were inconclusive due to large measurement errors in the 3ω method. Later, Wu *et al.* [13] measured the SPhP thermal conductivity of suspended SiN membranes dependent on temperature. However, they found no correlation between SPhP propagation lengths and thermal conductivity. In fact, early measurements were limited by the manufacture of nanoscale suspended membranes with large surface areas. Although a supported thin film structure is preferred for experimental validation and real-world application, for a polar dielectric thin film on a substrate (i.e., an asymmetric medium), the thickness of the film must be greater than the characteristic thickness d_c to have well-bounded behavior of the electromagnetic wave [6,15,16], which causes the contribution of the long-range surface mode to thermal conductivity to be greatly suppressed. Thus, no supported structure has shown surface-wave-enhanced heat conductivity.

Surface plasmon polaritons (SPPs) are additional electromagnetic waves associated with free electrons in metals that can be thermally excited and act as heat carriers. Thermally excited SPPs in lossy metals or heavily doped semiconductors exist in a broad spectral range and can be employed to tune the near-field thermal radiation [17–23]. In a thin metal layer, long-range SPPs can propagate across centimeters in the mid-infrared regime [8,24]. Thus, SPPs supported by the thin lossy metal film can significantly increase thermal conductivity. Here, we experimentally demonstrate that SPPs on a thin lossy metallic film can enhance its in-plane thermal conductivity even in a supported configuration, regardless of its thickness. Variable-radius Ti films are deposited on a glass substrate. The lateral size effect of SPP-enhanced thermal conductivity is clearly demonstrated at room temperature by limiting the SPPs' propagation to a smaller radius. Also, the film thickness effect is quantitatively analyzed. The measured in-plane thermal conductivity of Ti films is compared with a theoretical prediction to reveal the relationship between the SPP propagation length and thermal conductivity.

The in-plane thermal conductivity of Ti films was measured using a heat-dissipation-based steady-state thermoreflectance (SSTR) [25], as shown in Fig. 1(a). Section 1 of the Supplemental Material describes our SSTR setup and validation [26]. The SSTR has good measurement sensitivity on the in-plane thermal conductivity of thin films due

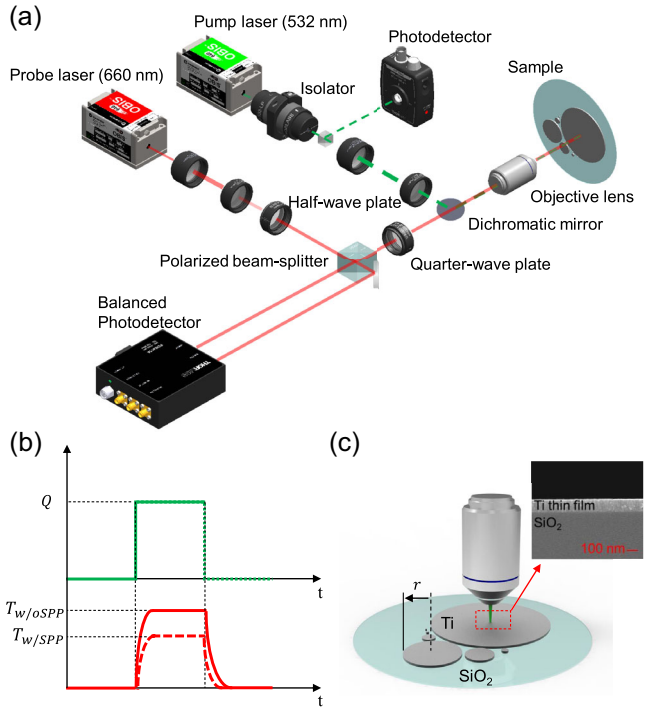

FIG. 1. Experimental setup for measuring the in-plane thermal conductivity of Ti films. (a) Schematic of a custom-built steady-state thermoreflectance setup. (b) Temperature rise at the sample surface corresponding to the applied laser irradiation with power Q. The rise of the temperature of the heated region drops if there exists a ballistic thermal transport via SPPs supported along a thin Ti film. (c) Schematic of a set of measurement samples. Ti films were patterned in circular shapes with different radius values r on a single glass (i.e., amorphous SiO_2) substrate. Inset shows the cross section of the deposited Ti film with a thickness of 100 nm.

to its long thermal penetration depth (see Fig. S2 of the Supplemental Material [26]). Fitting the measured temperature of the heated spot to the theoretical prediction from the two-dimensional (2D) heat diffusion model [33] yields the in-plane thermal conductivity of thin films (Section 3 of the Supplemental Material [26]). Considering its optical properties, we use the Ti film itself as a transducer [34]. Heat is mostly transferred through the Ti film like a suspended structure because the thermal conductivity of a glass substrate is much lower than that of Ti ($\sim$10 W/m $\cdot$ K; Table S2 [26]). We vary the lateral size of Ti film patterns to compare the temperature rise of a heated spot with respect to the propagation length of SPPs (i.e., thermal transport by SPPs). If heat is dissipated additionally via SPPs, the heated spot will show a lower temperature rise than the case without SPPs [Fig. 1(b)]. Using Fourier's law, the SPPs' "*effective*" thermal conductivity is calculated based on the heat flux [5]. Thus, the effective thermal conductivity of the SPPs, $k_{\parallel,\mathrm{spp}}$, indicates how much heat flux they can carry on a thin Ti film.

For measurements, thin Ti films (of different thicknesses) are e-beam deposited on a glass substrate and then circularly patterned by the liftoff process with a radius ranging from 200 μm to 28 mm. Ti films are uniformly deposited, as shown in the inset of Fig. 1(c). Due to the boundary scattering from Ti film patterns' radius, Matthiessen's rule is used to calculate SPPs' effective propagation length (i.e., $\Lambda_{\mathrm{eff}}^{-1} = \Lambda^{-1} + r^{-1}$, where r is the radius of the Ti film pattern). The spectral reflectance of the Ti film at wavelengths from 500 nm to 700 nm, which includes the pumping wavelength (i.e., $\lambda = 532$ nm) and the probing wavelength (660 nm), is measured with a UV-VIS spectrometer (UV-3600 Plus, Shimadzu) and agrees well with the theoretical prediction using the Drude model (Fig. S3 [26]). We use the Drude model parameters $\omega_\tau = 372\ \mathrm{cm}^{-1}$ and $\omega_p = 25\,000\ \mathrm{cm}^{-1}$ [35] for the Ti film. The imaginary part of its dielectric function is several orders of magnitude greater than SiO_2 [36] in the frequency range below 300 Trad/s.

Figure 2(a) shows the probe reflectance response ($\Delta V/V$) for Ti films of different thicknesses and radii. At a given thickness d, the Ti film with $r = 28$ mm has a significantly lower probe reflectance response than the one with $r = 200$ μm. For the 108.2 nm Ti film, $\Delta V/V$ is 5.3% lower at $r = 28$ mm than at 200 μm. When $r = 28$ mm, the heated spot's temperature rise is reduced by the same ratio as when $r = 200$ μm, because $\Delta V/V$ is proportional to it.

Considering that the probe reflectance response is proportional to the surface temperature rise ΔT, and the absorbed heat Q is proportional to the pump laser photodetector signal P, the proportionality constant γ can be defined as [25]

$$\left(\frac{\Delta V}{VP}\right) = \gamma\left(\frac{\Delta T(k)}{Q}\right). \tag{1}$$

The thermal conductivity k can be fitted to experimental data [i.e., $\Delta V/(VP)$] for a given γ by calculating $\Delta T(k)/Q$ based on the 2D heat diffusion model [33]. To determine the value of γ, one needs a calibration sample with known thermal conductivity (i.e., k_{cal}), i.e.,

$$\gamma = \left(\frac{\Delta T(k_{\mathrm{cal}})}{Q}\right)_{\mathrm{cal}}^{-1}\left(\frac{\Delta V}{VP}\right)_{\mathrm{cal}}, \tag{2}$$

where the subscript "cal" implies a calibration sample. In this Letter, the Ti film with the smallest radius (i.e., $r = 200$ μm) is used as the calibration sample because it has negligible SPP thermal conductivity [to be discussed in Fig. 2(b)]. To obtain γ from Eq. (2), the "*intrinsic*" thermal conductivity of the Ti film and glass substrate must be known. Due to its nanoscale thickness, the Ti film's thermal conductivity is anisotropic. The electronic contribution to in-plane thermal conductivity ($k_{\parallel,e}$) is calculated using four-probe measurement and the Wiedemann-Franz law (Sec. 5 of the Supplemental Material [26]). Because the

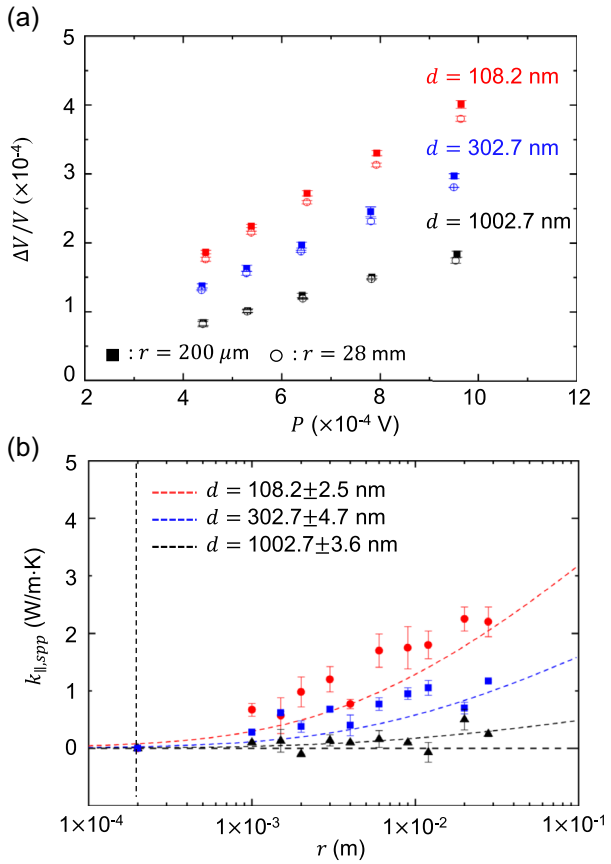

FIG. 2. SPP-enhanced thermal conductivity, $k_{\parallel,\mathrm{spp}}$. (a) Measured probe reflectance response with respect to the lock-in magnitude of the pump laser photodetector response for samples with different thicknesses and radii. Every plotted point was obtained by averaging the data over 5 seconds with a time interval of 50 ms. The standard deviation of each point is within 1.5%. (b) $k_{\parallel,\mathrm{spp}}$ of the Ti film with respect to the radius of the film. A sample with a radius of 200 μm was used for calibration; that is, we set $k_{\parallel,\mathrm{spp}} = 0$ with $r = 200$ μm for all samples. Every point is the averaged value of three repeated measurements, and dashed curves represent the theoretically predicted values of $k_{\parallel,\mathrm{spp}}$.

sample's radius is several orders of magnitude larger than the mean free path of an electron (∼10 nm [37]), the $k_{\parallel,e}$ values in Table S3 [26] are nearly independent of radius. The phononic contribution to the in-plane thermal conductivity of the Ti film ($k_{\parallel,ph}$) is obtained by multiplying the average value of the measured electronic contribution ($\overline{k_{\parallel,e}}$) from Table S3 of the Supplemental Material [26] by the ratio of phononic to electronic contribution [38]. The cross-plane thermal conductivity ($k_\perp$) of the Ti film is independently measured using the 3ω method (Fig. S5 [26]). Because of its low sensitivity to the heated spot temperature (Fig. S2 [26]), the interfacial thermal resistance (G) at the glass/Ti interface is adopted from Ref. [25]. Section 7 of the Supplemental Material describes the fitting procedure [26].

In-plane thermal conductivity can be calculated from measured $\Delta V/V$ values using the γ value. Note that the SSTR measures in-plane thermal conductivity ($k_\parallel$) by electrons, phonons, and SPPs. Thus, SSTR measurements yield $k_{\parallel,\mathrm{spp}}$ from $k_\parallel = \overline{k_{\parallel,e}} + k_{\parallel,ph} + k_{\parallel,\mathrm{spp}}$. Figure 2(b) plots the extracted $k_{\parallel,\mathrm{spp}}$ from SSTR measurements against a sample radius for three selected thicknesses of 108.2 nm, 302.7 nm, and 1002.7 nm. In Table S5 [26], a stylus profiler (Alpha-step 500, KLA TENCOR CORP) measures sample thicknesses. First, $k_{\parallel,\mathrm{spp}}$ in Fig. 2(b) has strong radius dependence except for the thickest sample. For example, a 108.2-nm-thick Ti film can increase $k_{\parallel,\mathrm{spp}}$ with $r = 28$ mm by about 25.0% when compared to a minimum of 200 μm. Electronic and phononic contributions cannot explain such a high enhancement due to their small mean free paths (<20 nm). For comparison, the theoretical prediction of $k_{\parallel,\mathrm{spp}}$ by the Boltzmann transport equation is also plotted in Fig. 2(b). SSTR measurements agree reasonably with the predicted $k_{\parallel,\mathrm{spp}}$, confirming the SPPs' contribution to the in-plane thermal conductivity. SPPs' long propagation lengths make $k_{\parallel,\mathrm{spp}}$ radius dependent. Figure 2(b) provides the first quantitative evidence for the ballistic nature of surface-polariton-enhanced in-plane thermal conductivity.

A Ti film thickness of 302.7 nm reduces $k_{\parallel,\mathrm{spp}}$ compared to $d = 108.2$ nm. At $r = 28$ mm, the 302.7-nm-thick Ti film has nearly half the $k_{\parallel,\mathrm{spp}}$ of the 108.2 nm film. If d increases further to 1002.7 nm, there exists no noticeable $k_{\parallel,\mathrm{spp}}$. The supported structure proposed in this Letter is clearly superior to the freestanding membrane structure for practical applications, because SPP thermal conductivity becomes significant only for nanoscale Ti films ($d \sim 100$ nm).

Enhancement of the in-plane thermal conductivity of the Ti film can be explained by thermal transport via SPPs along a thin Ti film based on kinetic theory with the Boltzmann transport equation [5,6], which leads to

$$k_{\parallel,\mathrm{spp}} = \frac{1}{4\pi d}\int_0^\infty k_\omega d\omega = \frac{1}{4\pi d}\int_0^\infty \hbar\omega\Lambda_{\mathrm{eff}}\beta_R\frac{df_0}{dT}d\omega, \tag{3}$$

where $\hbar$ is the Planck constant divided by 2π, ω is the angular frequency, β_R is the real part of the in-plane wave vector (i.e., $\beta = \beta_R + i\beta_I$), and f_0 is the Bose-Einstein distribution function. Because the propagation length of SPPs is defined by the imaginary part of the in-plane wave vector—i.e., $\Lambda = 1/(2\beta_I)$ [5,6]—which in turn leads to Λ_{eff}, one needs to solve the dispersion relation of SPPs supported by a thin Ti film deposited on a glass substrate [16,39]:

$$\tanh(p_{\mathrm{Ti}}d) = -\frac{p_{\mathrm{Ti}}\varepsilon_{\mathrm{Ti}}(p_a\varepsilon_s + p_s\varepsilon_a)}{p_{\mathrm{Ti}}^2\varepsilon_a\varepsilon_s + p_a p_s\varepsilon_{\mathrm{Ti}}^2}, \tag{4}$$

where a and s imply the air and substrate, respectively, and p_i is the cross-plane wave vector of the ith medium

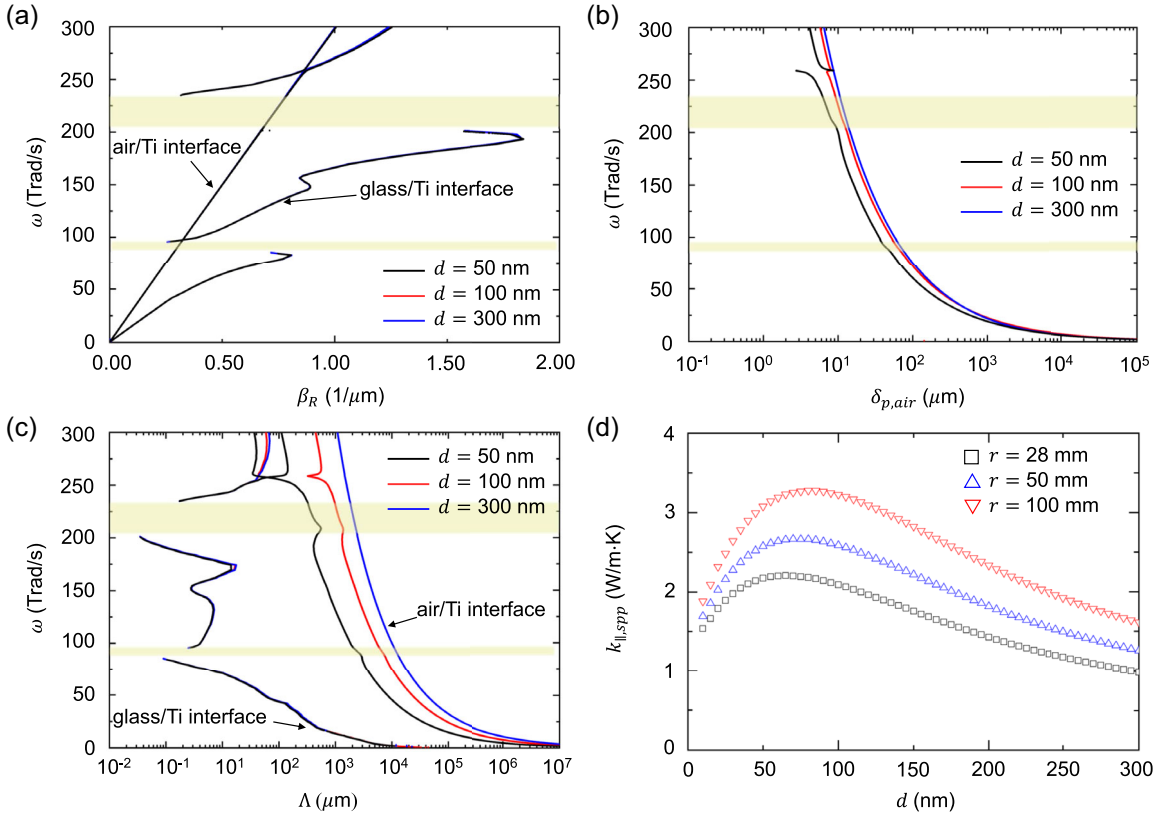

FIG. 3. SPP dispersion curves for Ti films on a glass substrate with film thicknesses $d = 50$ nm, 100 nm, and 300 nm. (a) Real part of in-plane wave vector (β_R). (b) Skin depth at air/Ti interface penetrating into air. (c) Propagation length (Λ) of SPP with respect to film thickness. The shaded region indicates the frequency range where the real part of the dielectric function of the glass substrate is negative. In other words, SPPs originating from a glass/Ti interface cannot be excited in the shaded region. (d) Calculated $k_{\|,\mathrm{spp}}$ with respect to the film thickness for different values of radius.

(i.e., $p_i^2 = \beta^2 - \varepsilon_i k_0^2$, with ε_i being the dielectric function of the medium i).

Figure 3(a) plots the real part of the in-plane wave vector β_R of Ti films deposited on glass substrates with $d = 50$, 100, and 300 nm. The dispersion curves are drawn for a frequency range from 0 to 300 Trad/s because the calculated spectral thermal conductivity of the Ti film on the glass substrate [i.e., $k_\omega = 1/(4\pi d)\hbar\omega\Lambda_{\mathrm{eff}}\beta_R(df_0/dT)$] has a considerable value at a frequency lower than 300 Trad/s, as shown in Fig. S8 [26]. In Fig. 3(a), two branches (i.e., symmetric and asymmetric modes) originate from the SPPs at two interfaces of the Ti film. For a metal film with asymmetric surrounding dielectrics, the symmetric SPP mode with a longer propagation length is supported at the interface between metal and dielectric with a lower refractive index (i.e., lower β_R at a given frequency) [8]. Because the air/Ti interface supports the symmetric mode that has a longer propagation length than the glass/Ti interface [Fig. 3(c)], the following discussion will be mainly focused on the SPPs at the air/Ti interface.

At the interface between semi-infinite air and semi-infinite Ti, a SPP dispersion follows the light line of air (i.e., photonlike behavior) in the sufficiently low-frequency region before reaching an asymptote at high frequency ($\sim\omega_p/\sqrt{2}$, with ω_p being the plasma frequency of Ti) [3]. Thermal transport via SPPs near the light line can also be observed by exact approach based on the fluctuational electrodynamics (see Secs. 10 and 11 of the Supplemental Material [26]). Although all of the β_R dispersion curves at the air/Ti interface look similar and coincide with the air light line regardless of the thickness of the Ti film in Fig. 3(a), there exists a slight difference near the air light line for different thicknesses of Ti films (see Fig. S11 [26]). As d decreases, the dispersion deviates from the air light line due to the coupling of the SPPs supported at the air/Ti interface and those at the glass/Ti interface. Importantly, the deviation of β_R from the light line leads to the confinement of SPPs at the interface. Figure 3(b) depicts the skin depth of SPPs from the air/Ti interface (i.e., the penetration depth into air) with respect to film thickness, where $\delta_{p,air} = 1/[2\mathrm{Re}(p_a)]$. As the separation between β_R and the light line becomes smaller, the field can penetrate deeper into the surrounding air, resulting in a longer propagation length, as in Fig. 3(c). Thus, SPPs with a long propagation length exist for thick Ti films where the SPPs at the air/Ti interface are located close to the light

line. Although not shown here, Λ with $d = 1000$ nm is essentially overlapped by that with $d = 300$ nm, suggesting that 300-nm-thick Ti film is already too thick for the coupling of SPPs at both interfaces. The penetration depth and the propagation length of surface plasmon on 300-nm-thick Ti film is also shown with the fluctuational electrodynamics (see Fig. S10 [26]).

For a freestanding SiO_2 membrane, surface waves propagate longer when the membrane is thinner [9]. Such discrepancies result from the different optical properties of a lossy metal and a polar dielectric. For a SiO_2 membrane, the Zenneck surface modes ($\epsilon_r > 0$ and $\epsilon_i > 0$, where ϵ_r and ϵ_i represent the real and imaginary parts of the permittivity of the thin film) dominate thermal conductivity by surface waves, while metal thin films can support SPPs (i.e., $\epsilon_r < -\epsilon_{\mathrm{air}}$) in a broad frequency range. Thus, the energy loss of surface waves decreases as film thickness decreases for the SiO_2 membrane, leading to a longer propagation length. Also, for a metal film surrounded by the same dielectrics, a symmetric SPP mode approaches the light line as the thickness of the metal film decreases and the coupling of SPPs at each metal/dielectric interface becomes significant [8,15], resulting in a longer propagation length of SPPs.

Contrarily, for a thin metal film on a dielectric substrate, SPPs can propagate longer along the interface when the film thickness is greater than the penetration depth of the metal film, so SPPs at the air/Ti interface can approach the air light line. In fact, when the analytic solution for the SPP dispersion at the single interface of semi-infinite metal/dielectric [8] is applied, the resulting dispersion is almost equal to that of a metal film with $d = 300$ nm (see Sec. 13 of the Supplemental Material [26]), indicating that the SPPs of each interface are nearly decoupled and show the characteristics of a semi-infinite metal/dielectric interface. In this structure, a 500-μm-thick glass (i.e., amorphous SiO_2) substrate can be assumed to be semi-infinite, because its thermal penetration depth is less than 10 μm ($\ll 500$ μm) when the beam diameter is less than 5 μm [33] (see Sec. 3 of the Supplemental Material [26]). Thus, for the considered Ti film on a glass substrate, there are essentially two interfaces: air/Ti and glass/Ti. The Zenneck modes for SiO_2 cannot occur at the glass/Ti interface simply because the adjacent medium to SiO_2 is not dielectric. For the same reason (i.e., the real part of Ti's dielectric function is always negative in the considered frequency region), the SPhPs for SiO_2 can not occur at the glass/Ti interface [10]. Therefore, we believe that the Zenneck and SPhP modes for the glass substrate do not play any role in the measurements.

At low frequencies below 100 Trad/s, the SPP propagation lengths can be longer than 1 cm, causing the radius dependence of $k_{\parallel,\mathrm{spp}}$ in Fig. 2(b). Considering that the effective propagation length of SPP is given by $\Lambda_{\mathrm{eff}}^{-1} = \Lambda^{-1} + r^{-1}$, the radius of samples mostly limits low-frequency SPPs under 100 Trad/s if $r < 1$ cm. Equation (3) also suggests that $1/(4\pi d)$ also determines the SPP thermal conductivity. This is the reason why the 302.7-nm-thick Ti film has a lower $k_{\parallel,\mathrm{spp}}$ than the 108.2-nm-thick Ti film even though it has a longer Λ. In other words, the contribution of thermal conduction via SPPs can be substantial in thin films, although the SPPs can propagate longer for thicker films, implying the existence of an optimum thickness for SPP-enhanced thermal conductivity.

Figure 3(d) shows the calculated $k_{\parallel,\mathrm{spp}}$ for Ti film thickness when $r = 28$ mm, 50 mm, and 100 mm. Due to the interplay between $1/(4\pi d)$ and $\beta_R \Lambda_{\mathrm{eff}}$ in Eq. (3), the optimal thickness exists at a given radius. The optimal thickness for a glass-deposited Ti film is 70 nm. As d decreases below 70 nm, the coupling of SPPs at both interfaces reduces SPP propagation length, decreasing $k_{\parallel,\mathrm{spp}}$. However, as d increases beyond 70 nm, $1/(4\pi d)$ will decrease $k_{\parallel,\mathrm{spp}}$. Because the radiation penetration depth of Ti is approximately 40 nm in the infrared spectral region (<200 Trad/s), the coupling of SPPs may occur up to $d \sim 120$ nm.

Finally, SSTR measurements of the supported Ti film on a glass substrate show that surface-polariton-enhanced in-plane thermal conductivity is dependent on the thickness and lateral size. When $r = 28$ mm, the 108.2-nm-thick Ti film exhibits a $k_{\parallel,\mathrm{spp}}$ value about 25% of its intrinsic value. Due to broadband SPPs supported at an air/lossy metal interface, an optimal thickness exists for the maximum $k_{\parallel,\mathrm{spp}}$. This Letter introduces a supported metal thin film configuration that uses a surface polariton to enhance in-plane thermal conductivity, which is nearly impossible for polar-dielectric counterparts.

This research is supported by the Basic Science Research Program (No. NRF-2020R1A4A4078930) through the National Research Foundation of Korea (NRF) funded by the Ministry of Science and ICT.

*mklim@kimm.re.kr
†bongjae.lee@kaist.ac.kr

[1] T. Qiu and C. Tien, J. Heat Transf. **115**, 835 (1993).
[2] Z. M. Zhang, *Nano/Microscale Heat Transfer* (Springer, New York, 2007).
[3] H. Raether, *Surface Plasmons on Smooth and Rough Surfaces and on Gratings* (Springer-Verlag, Berlin, 1988).
[4] J.-P. Mulet, K. Joulain, R. Carminati, and J.-J. Greffet, Appl. Phys. Lett. **78**, 2931 (2001).
[5] Dye-Zone A. Chen, A. Narayanaswamy, and G. Chen, Phys. Rev. B **72**, 155435 (2005).
[6] J. Ordonez-Miranda, L. Tranchant, T. Tokunaga, B. Kim, B. Palpant, Y. Chalopin, T. Antoni, and S. Volz, J. Appl. Phys. **113**, 084311 (2013).
[7] S. Gluchko, B. Palpant, S. Volz, R. Braive, and T. Antoni, Appl. Phys. Lett. **110**, 263108 (2017).

[8] J. J. Burke, G. I. Stegeman, and T. Tamir, Phys. Rev. B **33**, 5186 (1986).
[9] L. Tranchant, S. Hamamura, J. Ordonez-Miranda, T. Yabuki, A. Vega-Flick, F. Cervantes-Alvarez, J. J. Alvarado-Gil, S. Volz, and K. Miyazaki, Nano Lett. **19**, 6924 (2019).
[10] K. Joulain, J.-P. Mulet, F. Marquier, R. Carminati, and J.-J. Greffet, Surf. Sci. Rep. **57**, 59 (2005).
[11] D.-Z. A. Chen and G. Chen, Front. Heat Mass Transf. **1**,023005 2010).
[12] G. Baffou, C. Girard, and R. Quidant, Phys. Rev. Lett. **104**, 136805 (2010).
[13] Y. Wu, J. Ordonez-Miranda, S. Gluchko, R. Anufriev, D. D. S. Meneses, L. Del Campo, S. Volz, and M. Nomura, Sci. Adv. **6**, eabb4461 (2020).
[14] D.-Z. A. Chen and G. Chen, Appl. Phys. Lett. **91**, 121906 (2007).
[15] F. Yang, J. R. Sambles, and G. W. Bradberry, Phys. Rev. B **44**, 5855 (1991).
[16] M. Lim, J. Ordonez-Miranda, S. S. Lee, B. J. Lee, and S. Volz, Phys. Rev. Appl. **12**, 034044 (2019).
[17] S. Basu and M. Francoeur, Appl. Phys. Lett. **98**, 113106 (2011).
[18] S.-A. Biehs, M. Tschikin, and P. Ben-Abdallah, Phys. Rev. Lett. **109**, 104301 (2012).
[19] R. Messina and P. Ben-Abdallah, Sci. Rep. **3**, 1383 (2013).
[20] X. Liu, R. Zhang, and Z. Zhang, Int. J. Heat Mass Transfer **73**, 389 (2014).
[21] S. Jin, M. Lim, S. S. Lee, and B. J. Lee, Opt. Express **24**, A635 (2016).
[22] M. Lim, J. Song, J. Kim, S. S. Lee, I. Lee, and B. J. Lee, J. Quant. Spectrosc. Radiat. Transfer **210**, 35 (2018).
[23] M. Lim, J. Song, S. S. Lee, and B. J. Lee, Nat. Commun. **9**, 1 (2018).
[24] P. Berini, Adv. Opt. Photonics **1**, 484 (2009).
[25] J. L. Braun, D. H. Olson, J. T. Gaskins, and P. E. Hopkins, Rev. Sci. Instrum. **90**, 024905 (2019).
[26] See Supplemental Material at http://link.aps.org/supplemental/10.1103/PhysRevLett.130.176302 for (1) Validation of experimental setup, (2) Sensitivity analysis of SSTR, (3) Summary of thermal properties used in a 2D heat diffusion model, (4) Optical property of Ti film, (5) Electron contribution of in-plane thermal conductivity of Ti film ($k_{\parallel,e}$) measured by four-probe measurement, (6) Measurement of the cross-plane thermal conductivity of Ti film by using the 3ω method, (7) Fitting procedure and uncertainty of $k_{\parallel,\mathrm{spp}}$ obtained by SSTR method, (8) Measurement of Ti film thickness with stylus profiler, (9) Spectral thermal conductivity of SPP, (10) Fluctuational electrodynamics, (11) Thermal conductance calculated via fluctuationalal electrodynamics, (12) Dispersion curve near the light line of air, (13) Analytic solution of SPP, (14) Beam diameter of probe and pump laser, and (15) Thermal conductivity of glass substrate, which includes Refs. [27–32].
[27] T. Borca-Tasciuc, A. Kumar, and G. Chen, Rev. Sci. Instrum. **72**, 2139 (2001).
[28] G. Matsui and H. Kato, Rev. Sci. Instrum. **82**, 034905 (2011).
[29] N. W. Ashcroft and N. D. Mermin, *Solid State Physics* (Harcourt College, New York, 1976).
[30] JCGM 100:2008, Evaluation of measurement data - Guide to the expression of uncertainty in measurement, https://www.bipm.org/documents/20126/2071204/JCGM_100_2008_E.pdf/cb0ef43f-baa5-11cf-3f85-4dcd86f77bd6.
[31] C. Fu and Z. Zhang, Int. J. Heat Mass Transfer **49**, 1703 (2006).
[32] J. Yang, C. Maragliano, and A. J. Schmidt, Rev. Sci. Instrum. **84**, 104904 (2013).
[33] J. L. Braun and P. E. Hopkins, J. Appl. Phys. **121**, 175107 (2017).
[34] B. Abad, D.-A. Borca-Tasciuc, and M. Martin-Gonzalez, Renewable Sustainable Energy Rev. **76**, 1348 (2017).
[35] M. A. Ordal, R. J. Bell, R. W. Alexander, L. A. Newquist, and M. R. Querry, Appl. Opt. **27**, 1203 (1988).
[36] E. D. Palik, *Handbook of Optical Constants of Solids* (Academic Press, New York, 1998), Vol. 3.
[37] M. Day, M. Delfino, J. Fair, and W. Tsai, Thin Solid Films **254**, 285 (1995).
[38] Z. Tong, S. Li, X. Ruan, and H. Bao, Phys. Rev. B **100**, 144306 (2019).
[39] J. Ordonez-Miranda, L. Tranchant, Y. Chalopin, T. Antoni, and S. Volz, J. Appl. Phys. **115**, 054311 (2014).